Eur. Phys. J. B (2013) 86: 226
DOI: 10.1140/epjb/e2013-31011-y

THE EUROPEAN PHYSICAL JOURNAL B

Regular Article

Facile growth of monolayer MoS_2 film areas on SiO_2

John Mann[1], Dezheng Sun[1,2], Quan Ma[1], Jen-Ru Chen[1], Edwin Preciado[1], Taisuke Ohta[3], Bogdan Diaconescu[3], Koichi Yamaguchi[1], Tai Tran[1], Michelle Wurch[1], KatieMarie Magnone[1], Tony F. Heinz[2], Gary L. Kellogg[3], Roland Kawakami[1], and Ludwig Bartels[1,a]

[1] Chemistry, Physics, and Materials Science and Engineering, University of California, CA 92521 Riverside, USA
[2] Departments of Physics and Electrical Engineering, Columbia University, NY 10027 New York, USA
[3] Sandia National Laboratories, 87185 Albuquerque, New Mexico, USA

Received 6 November 2012 / Received in final form 11 February 2013
Published online 20 May 2013 –

Abstract. Areas of single-layer MoS_2 film can be prepared in a tube furnace without the need for temperature control. The films were characterized by means of Raman spectroscopy, photoluminescence, low-energy electron diffraction and microscopy, and X-ray photoelectron spectroscopy and mapping. Transport measurements show n-doped material with a mobility of 0.26 $cm^2\ V^{-1}\ s^{-1}$.

Molybdenum disulfide, MoS_2, has attracted widespread attention as a material that can be prepared in a stable form down to the single-layer limit. As a monolayer, the material becomes a direct-gap semiconductor with a gap of 1.8 eV [1,2]. Single-layer MoS_2 transistors have been reported with mobilities on the order of 1 $cm^2\ V^{-1}\ s^{-1}$ and beyond [3–6], as well as on-off ratios up to 10^8 at room temperature. Bulk MoS_2 and most mono- or few layer MoS_2 materials examined to date exhibit n-doped behavior [3–9], but p-doped behavior has also been reported [10]; the use of gating with an ionic liquid has permitted access to ambipolar operation [11]. Phototransistors made of single-layer MoS_2 show reasonable switching behavior (∼50 ms) and stable performance [8]. More recently, MoS_2 has also been shown as a candidate for valleytronics devices, and dynamic valley polarization has been achieved by excitation with circularly-polarized light [12–16].

Apart from mechanical exfoliation [17], MoS_2 monolayers can be fabricated by chemical vapor deposition (CVD) based growth on Cu [18], Au [10,19–21], SiO_2 [10,22], and various other insulators [6,10,23]. In addition to MoS_2 film areas, several other forms of MoS_x have been reported, including MoS nanowires [24,25] and Mo_2S_3 films [26,27]. Here, we show that the preparation of MoS_2 can be achieved in a very facile manner. Prior MoS_2 growth started from thin Mo layers [10] prepared by physical vapor deposition (PVD) or dip-coating of a substrate in a Mo-containing solution [6] followed by sulfurization. Another promising approach involves the simultaneous deposition of molybdenum (typically from a MoO_3 source) and elemental sulfur [22]. In this manuscript, we follow the latter method and show that continuous films hundreds of microns across can be achieved with minimal control of the growth conditions.

Our films are found to be uniform in their spectroscopic properties and feature large areas that are of monolayer thickness. In this manuscript, we provide photoluminescence (PL), Raman spectroscopy, low-energy electron diffraction (LEED) and microscopy (LEEM), X-ray photoelectron spectroscopy (XPS), atomic force microscopy (AFM) imaging and transport measurements to validate the quality of our films.

Our growth process for MoS_2 monolayers is based on the solid-source scheme of Lee et al. [22]. We use two alumina crucibles (Aldrich Z561738, 70 mm×14 mm×10 mm) containing MoO_3 (Aldrich 99.5%) and sulfur (Alfa 99.5%) powders as our Mo and S sources, respectively. These sources are placed in a quartz process tube (2" diameter), which is inserted in a furnace (Mellen TT12), only the center zone of which is powered. A rapid flow of nitrogen gas (99.999%) is used to purge the tube (5.0 SCFH, 0.14 Nm^3/h)), with subsequent film growth occurring at a reduced nitrogen flow rate (0.5 SCFH, 0.014 Nm^3/h). The crucible containing MoO_3 is placed at the center of the heated zone, with the substrate resting directly on it. The crucible containing sulfur is placed upstream, outside the zone of the tube furnace that was heated. Our substrate is a 3 × 3 cm piece of a boron-doped Si (110) wafer covered by a 300 nm thick layer of oxide (SUMCO). The substrate is cleaned immediately prior to growth by a piranha etch solution, formed as a mixture of 3 parts sulfuric acid and 1 part hydrogen peroxide (30%). We also applied an O_2 plasma etch to some substrates; we found similar results to those for the unprocessed substrates. We optimized the position of the sulfur crucible

[a] e-mail: bartels@ucr.edu

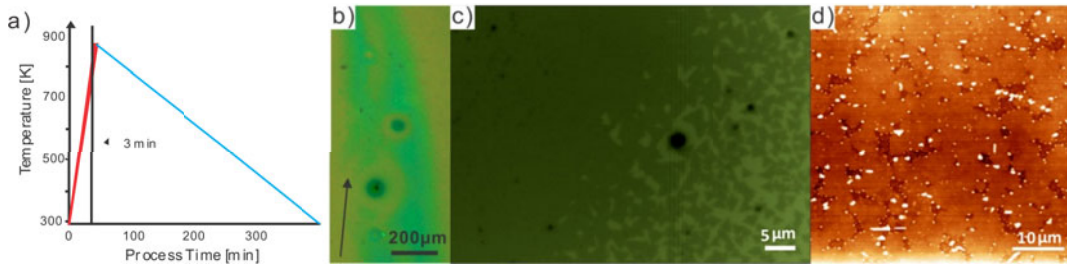

Fig. 1. (a) Approximate temperature transient during MoS_2 growth. The furnace is powered until 3 min after the sulfur is molten and subsequently switched off. (b) Optical microscope image taken with neutral color balance filter of the MoS_2 film (light green) on the substrate. The direction of the N_2 is indicated by an arrow. The circular feature is an area of multilayer MoS_2. (c) At its edge, the MoS_2 film (dark area) transitions into an array of individual MoS_2 islands, mostly of triangular form. (d) AFM imaging showing that the continuous film has a small number of irregularly shaped pits. No domain boundaries were identified.

so that during heat-up the sulfur melts to form a flat, uniform liquid surface at the time that the center section of the process tubes (where the MoO_3 crucible is located) reaches ∼880 K, as measured by a type-K thermocouple at the outer surface of the process tube. We find that the duration that the substrate is exposed to vapor from the liquid sulfur is crucial in determining the structures that we grow. We achieved the growth described in this manuscript by waiting and continuing to power the center section of the furnace for 3 min after the sulfur melts. Subsequently, all power to the furnace is switched off and it is left to cool undisturbed, while the N_2 flow is continued. Thus, no temperature control of the furnace is required. Figure 1a shows the temperature transient.

After deposition, the substrates display elongated areas hundreds of microns long and approximately 100 microns across (Fig. 1b) that are continuously covered by a MoS_2 film. The long axes of these areas are aligned with the nitrogen flow during growth. In the following, we present spectroscopic evidence that identifies these areas as single-layer MoS_2. At the edges, these areas are surrounded by isolated islands, mostly triangular in shape (Fig. 1c), which exhibit spectroscopic and topographic characteristics identical to the film (*vide infra*). In contrast, other regions of the substrate are covered by triangular multilayer MoS_2 islands or show no deposited material at all. We also find thicker MoS_2 films predominantly surrounding areas with substrate point defects, such as the dark circles in Figures 1b and 1c.

AFM shows that the film and the islands at its edge are homogeneous in height; no steps in height are found except for a small number of isolated irregular pits. No dislocation lines or 2D grain boundaries were resolved by AFM.

LEED measurements from the film reveal a hexagonal pattern commensurate with the lattice vectors of MoS_2. The orientation of the LEED pattern varies across the film. Dark-field LEEM imaging [28] was used to collect electrons from the (01) LEED spot at different rotational angles. Figures 2a and 2b show two such images obtained for ∼10° rotation (our azimuthal acceptance angle was about ±5° each time). Areas of the film appear at different brightness depending on whether or not one of the MoS_2 (01) LEED spots is angularly aligned with the diffraction aperture position. This provides direct evidence of the domain crystallinity, orientation, and size. Most domains are found to be 3–5 μm in size.

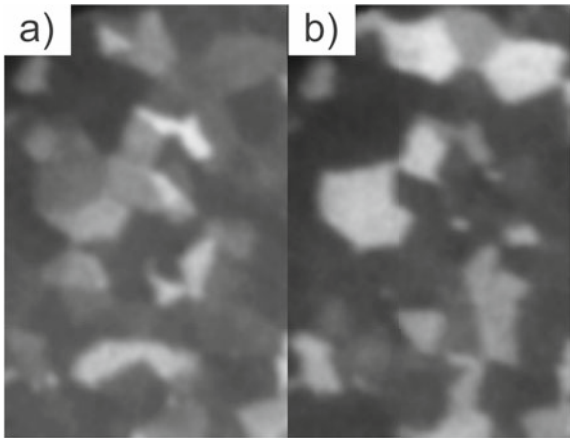

Fig. 2. (a, b) Spatial distribution of intensity from the MoS_2 (01) diffraction spot at two angular orientations ∼10° apart. The MoS_2 monolayer domains appear with different brightness depending on their angular orientation. Image size: 18 × 28 μm^2.

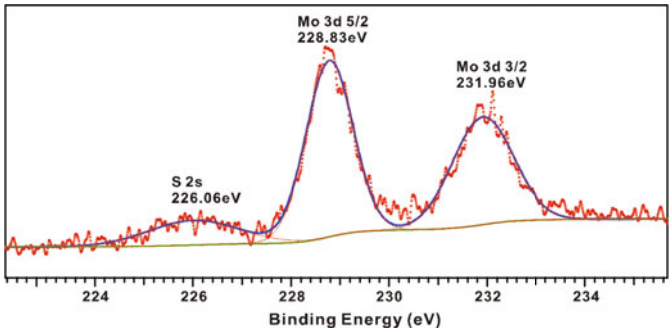

Fig. 3. XPS of the Mo 3*d* and S 2*s* peaks from the MoS_2 films on the SiO_2/Si substrate.

Selected area XPS measurements of the film using a Mg K-α source and a VG Scienta R3000 analyzer (Fig. 3) show the sulfur 2*s* and molybdenum 3*d* 5/2 and 3/2 peaks

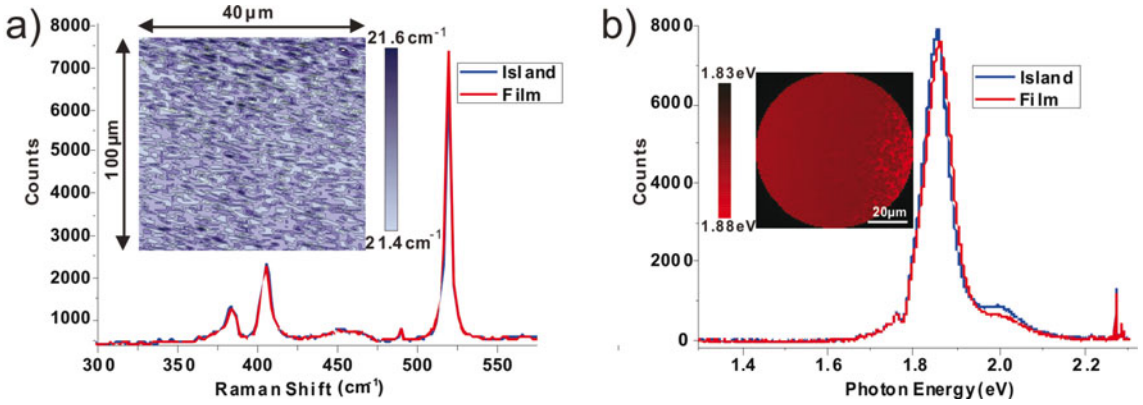

Fig. 4. (a) Raman spectra of the continuous MoS_2 film and of the region with island structures. Two characteristic peaks are located at Raman shifts of 384.3 and 405.2 cm^{-1} corresponding, respectively, to the MoS_2 E^1_{2g} and A_{1g} vibrational modes. The inset shows mapping of the frequency difference between the E^1_{2g} and A_{1g} modes. The variation of $\leqslant$0.2 cm^{-1} is indicative of the high uniformity of the film. (b) Photoluminescence spectra of the continuous MoS_2 film (red) and of a triangular island at the film's edge (blue). Both spectra exhibit a single peak at 1.87 eV. The inset displays mapping data from the continuous film (left) to an area covered partly by islands (right).

at 226.1, 228.8, and 232.0 eV, respectively. These core-level binding energies suggest the charge states of S^{2-} and Mo^{4+}. Referencing the spectrum to the silicon peaks of the substrate, we find peak positions in good agreement to those previously reported for bulk MoS_2 [29]. Although some areas of the sample exhibited peaks/shoulders corresponding to a higher oxidation state of molybdenum (Mo^{6+}, indicative of MoO_3) as shown in reference [10], these features were absent in the region of the continuous film area and the monolayer islands. These measurements confirm that the films we produce are comprised of pure MoS_2.

For Raman spectroscopy (Fig. 4a), we used a 532 nm cw laser with a power of 0.1 mW in a spot size of 1 μm. The spectrum shows the E^1_{2g} and A_{1g} peaks of MoS_2 at 384 and 405 cm^{-1}, respectively, and the peak of the silicon substrate at 520 cm^{-1}. The separation of the E^1_{2g} and A_{1g} peaks can be used to identify the MoS_2 film thickness. We find a value of 21.5 cm^{-1}, which is in good agreement with prior measurements on CVD-grown MoS_2 [6,10,22,30] and lies between the values observed for monolayers and bilayers of exfoliated MoS_2 [31]. The positions of the Raman peaks and their separation is uniform across our film areas. Mapping the sample in a 1 μm grid, we observe variations $\leqslant$0.3 cm^{-1} over a region with a size >100 μm (inset in Fig. 4a); the islands at the edge of the film area exhibit Raman features identical to those in the center of the film.

PL measurements (Fig. 4b) were performed with the same laser excitation source and conditions as for Raman spectroscopy. We find a single emission peak at a photon energy of 1.87 eV. This peak corresponds to the direct-gap transition of monolayer MoS_2 [1,2]. The photoluminescence yield was about twice as high as what we find for MoS_2 monolayers exfoliated on SiO_2. The continuous film and the area consisting of individual islands show the same photoluminescence characteristics.

We measured the I-V characteristics (Fig. 5) in a 4-point probe setup across a 2 μm gap as a function of a gate voltage applied to the silicon substrate. The results

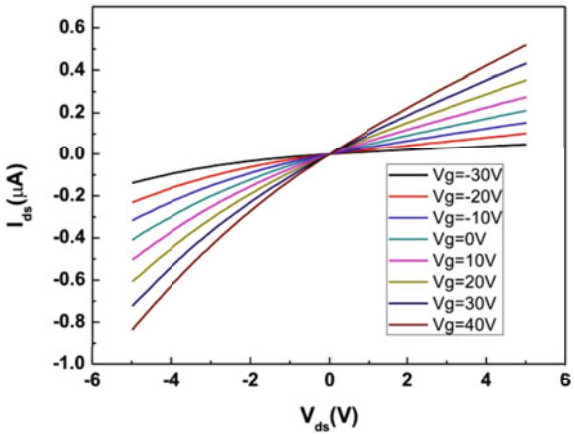

Fig. 5. Current-voltage (I-V) measurements in a 4-probe setup across a 2 μm gap at the edge of our monolayer MoS_2 film as a function of gate voltage V_g. The conductivity increases for positive gate voltages, indicating n-type material.

reveal n-doped material, as is typically found for both exfoliated and deposited MoS_2 films [3–9]. We speculate that this behavior is caused by sulfur vacancies in the film and that further optimization of the growth process can reduce their density. Application of gate voltages up to –100 V (for a nominal oxide thickness of 300 nm) was insufficient to render the device ambipolar. We measured a room-temperature mobility of 0.26 $cm^2\ V^{-1}\ s^{-1}$, comparable to results of many previous measurements of similar MoS_2 samples [3–6].

In summary, we have shown the possibility of growing large-area MoS_2 films using a simple solid-source deposition scheme, without the need for temperature control. The resultant films show monolayer behavior and excellent uniformity in their photoluminescence and Raman signals. Future research will address the chemical and catalytic properties of these films.

We gratefully acknowledge support from the US National Science Foundation (UCR, Columbia University: DMR 1106210) for novel methods of the growth of MoS_2 and related films. XPS and Raman characterization of the films was supported by a grant by the US Department of Energy (UCR, Columbia University: DE-FG02-07ER15842). Electrical characterization was funded by the Army Research Office under Grant W911NF-11-1-0182 (UCR). LEEM investigations were performed at the Center for Integrated Nanotechnologies, an Office of Science User Facility operated for the U.S. Department of Energy (DOE) Office of Science. BD and TO were supported by the US DOE BES Division of Materials Science and Engineering. Sandia National Laboratories is a multi-program laboratory managed and operated by Sandia Corporation, a wholly owned subsidiary of Lockheed Martin Corporation, for the U.S. Department of Energy's National Nuclear Security Administration under contract DE-AC04-94AL85000.

References

1. K.F. Mak, C. Lee, J. Hone, J. Shan, T.F. Heinz, Phys. Rev. Lett. **105**, 136805 (2010)
2. A. Splendiani, L. Sun, Y. Zhang, T. Li, J. Kim, C.-Y. Chim, G. Galli, F. Wang, Nano Lett. **10**, 1271 (2010)
3. B. Radisavljevic, A. Radenovic, J. Brivio, V. Giacometti, A. Kis, Nat. Nanotech. **6**, 147 (2011)
4. S. Ghatak, A.N. Pal, A. Ghosh, ACS Nano **5**, 7707 (2011)
5. D.J. Late, B. Liu, H.S.S.R. Matte, V.P. Dravid, C.N.R. Rao, ACS Nano **6**, 5635 (2012)
6. K.-K. Liu et al., Nano Lett. **12**, 1538 (2012)
7. H. Li, Z. Yin, Q. He, H. Li, X. Huang, G. Lu, D.W.H. Fam, A.I.Y. Tok, Q. Zhang, H. Zhang, Small **8**, 63 (2012)
8. Z. Yin, H. Li, H. Li, L. Jiang, Y. Shi, Y. Sun, G. Lu, Q. Zhang, X. Chen, H. Zhang, ACS Nano **6**, 74 (2011)
9. A. Ayari, E. Cobas, O. Ogundadegbe, M.S. Fuhrer, J. Appl. Phys. **101**, 014507 (2007)
10. Y. Zhan, Z. Liu, S. Najmaei, P.M. Ajayan, J. Lou, Small **8**, 966 (2012)
11. Y. Zhang, J. Ye, Y. Matsuhashi, Y. Iwasa, Nano Lett. **12**, 1136 (2012)
12. D. Xiao, G.-B. Liu, W. Feng, X. Xu, W. Yao, Phys. Rev. Lett. **108**, 196802 (2012)
13. H. Zeng, J. Dai, W. Yao, D. Xiao, X. Cui, Nat. Nanotech. **7**, 490 (2012)
14. K.F. Mak, K. He, J. Shan, T.F. Heinz, Nat. Nanotech. **7**, 494 (2012)
15. T. Cao et al., Nat. Commun. **3**, 887 (2012)
16. T. Cao, J. Feng, J. Shi, Q. Niu, E. Wang, `arXiv:1112.4013 [cond-mat.mtrl-sci]` (2012)
17. K. Novoselov, D. Jiang, F. Schedin, T. Booth, V. Khotkevich, S. Morosov, A. Geim, Proc. Natl. Am. Soc. **102**, 10454 (2005)
18. D. Kim, D. Sun, W. Lu, Z. Cheng, Y. Zhu, D. Le, T.S. Rahman, L. Bartels, Langmuir **27**, 11650 (2011)
19. J.V. Lauritsen et al., J. Catal. **249**, 220 (2007)
20. S. Helveg, J. Lauritsen, E. Laegsgaard, I. Stensgaard, J. Norskov, B. Clausen, H. Topsoe, F. Besenbacher, Phys. Rev. Lett. **84**, 951 (2000)
21. T.F. Jaramillo, K.P. Jørgensen, J. Bonde, J.H. Nielsen, S. Horch, I. Chorkendorff, Science **317**, 100 (2007)
22. Y.-H. Lee et al., Adv. Mater. (2012)
23. J. Kibsgaard, B.S. Clausen, H. Topsøe, E. Lægsgaard, J.V. Lauritsen, F. Besenbacher, J. Catal. **263**, 98 (2009)
24. J. Kibsgaard, A. Tuxen, M. Levisen, E. Laegsgaard, S. Gemming, G. Seifert, J.V. Lauritsen, F. Besenbacher, Nano Lett. **8**, 3928 (2008)
25. I. Vilfan, Eur. Phys. J. B **51**, 277 (2006)
26. D. Sun et al., Angew. Chem. **124**, 10430 (2012)
27. R.K. Tiwari, J.S. Yang, M. Saeys, C. Joachim, Surf. Sci. **602**, 2628 (2008)
28. J.T. Robinson, S.W. Schmucker, C.B. Diaconescu, J.P. Long, J.C. Culbertson, T. Ohta, A.L. Friedman, T.E. Beechem, ACS Nano **7**, 637 (2013)
29. NIST, (National Institute of Standards and Technology, Gaithersburg, MD, 1989)
30. S. Balendhran, J.Z. Ou, M. Bhaskaran, S. Sriram, S. Ippolito, Z. Vasic, E. Kats, S. Bhargava, S. Zhuiykov, K. Kalantar-zadeh, Nanoscale **4**, 461 (2012)
31. C. Lee, H. Yan, L.E. Brus, T.F. Heinz, J. Hone, S. Ryu, ACS Nano **4**, 2695 (2010)